Efficient Light Harvesting with Micropatterned 3D Pyramidal Photoanodes in Dye-Sensitized Solar Cells

Sanghyuk Wooh, Hyunsik Yoon, Jae-Hyun Jung, Yong-Gun Lee, Jai Hyun Koh, Byoungho Lee, Yong Soo Kang, and Kookheon Char**

Renewable energy resources have recently gained a great deal of attention due to the ever increasing energy demand, the shortage of fossil fuels, and the growing interest in ecofriendly energy sources. In the field of renewable energy, solar cells have been regarded as a good candidate because they can utilize sunlight as an unlimited energy source. In recent years, the light trapping or harvesting in photovoltaic devices has been extensively explored because of the needs for the reduction of active material thickness to overcome the intrinsic limitations associated with diffusional path length for charge carriers and the charge-carrier recombination occurring through interfaces.[1–10] Light absorbance generally decreases as the film thickness of a light absorbing active layer decreases, resulting in a low energy-conversion efficiency. There have been many trials to harvest light efficiently in order to compensate for lack of light absorption due to the reduction in the film thickness of the active layer.[4–10] In other words, the light-trapping strategy could be quite useful to improve the power conversion efficiency for the limited film thickness of thin-film photovoltaic devices such as dye-sensitized solar cells (DSCs)[11,12] and organic photovoltaics (OPVs).[13] For example, inverse opal nanostructures,[14–16] scattering layers on top of active layer,[17,18] and plasmonics with metallic nanostructures[4,19] have been developed for trapping incident light inside the photoanodes of DSCs. Also, nanopatterned photoanodes obtained from etched transparent conducting glasses[20,21] and a nanoimprinted neutral paste on the active layer[22] have been introduced. However, since the previous approaches have some limitations such as electron diffusion problem and low dye adsorption, we are still eager to optimize the light absorbance within the active layer for the maximal efficiency of devices in order to compete with conventional textured silicon solar cells.[2,3]

Here, we demonstrate a light-trapping strategy in DSCs with 3D photoanodes made from 20 nm TiO_2 nanoparticles, employed for common photosensitizing layers. In order to fabricate 3D TiO_2 photoanodes, we exploited the soft lithographic technique, so called soft molding, with poly(dimethyl siloxane) (PDMS) molds.[23] In the present study, 3D TiO_2 photoanodes with different geometries are fabricated by adopting the soft-molding technique, and their optical and photovoltaic properties are investigated in detail. Over 20% enhancement in light absorption, as well as in the photocurrent of DSCs, have been achieved by changing the architecture of the TiO_2 photoanodes from 2D flat surfaces to 3D pyramids, due to the total reflection of incident light on the facets of the pyramid structures. For a low-cost fabrication, we propose an economical approach of preparing the optimized master by use of the conventional silicon wet-etching process to construct the pyramidal photoanodes. Furthermore, the combination of a 3D photoanode with a scattering layer, which is conventionally used to effectively trap light, shows a remarkable enhancement of light absorption as well as photocurrent generation.[24,25]

Figure 1a shows a schematic illustration of the fabrication of the 3D TiO_2 photoanodes by the soft-molding method, which is a type of soft-lithography technique.[23] A PDMS mold was employed to absorb the evaporated solvent of a TiO_2 paste while filling the TiO_2 paste into the void space of the mold. After preparing the master by conventional photolithography or a micromachining technique, we made replica molds from the masters with either polyurethane acrylate (PUA) (301RM, Minuta Tech)[26] or PDMS. We used the PDMS precursor at a mixing ratio of 10:1 (precursor:curing agent) and cured it at 60 °C for 10 h. The cured PDMS molds were removed by hand and cut prior to use. In order to prepare the inverted pyramid structures of TiO_2, PUA molds were first replicated from the original master, followed by the PDMS molding with the replicated PUA.

We prepared patterned photoanodes of DSCs by first layering electron-blocking layers on fluorine-doped tin oxide (FTO) substrates and then coating with a highly viscous TiO_2 paste by the doctor-blade method to yield a film thickness of about 7 μm. After gently pressing the TiO_2 paste film at room

S. Wooh,[+] J. H. Koh, Prof. K. Char
The National Initiative Creative Research Center for Intelligent Hybrids & the World Class University Program for Chemical Convergence for Energy and Environment
School of Chemical and Biological Engineering
Seoul National University
Seoul 151-744, Korea
E-mail: khchar@plaza.snu.ac.kr
Prof. H. Yoon[+]
Department of Chemical and Biomolecular Engineering
Seoul National University of Science & Technology
Seoul 139-743, Korea
Dr. J.-H. Jung, Prof. B. Lee
The National Creative Research Center for Active Plasmonics Application Systems, School of Electrical Engineering
Seoul National University
Seoul 151-774, Korea
Dr. Y.-G. Lee, Prof. Y. S. Kang
The WCU Department of Energy Engineering and Center for Next Generation Dye-Sensitized Solar Cells
Hanyang University
Seoul 133-791, Korea
E-mail: kangys@hanyang.ac.kr
[+] These authors contributed equally to this work.

DOI: 10.1002/adma.201300085

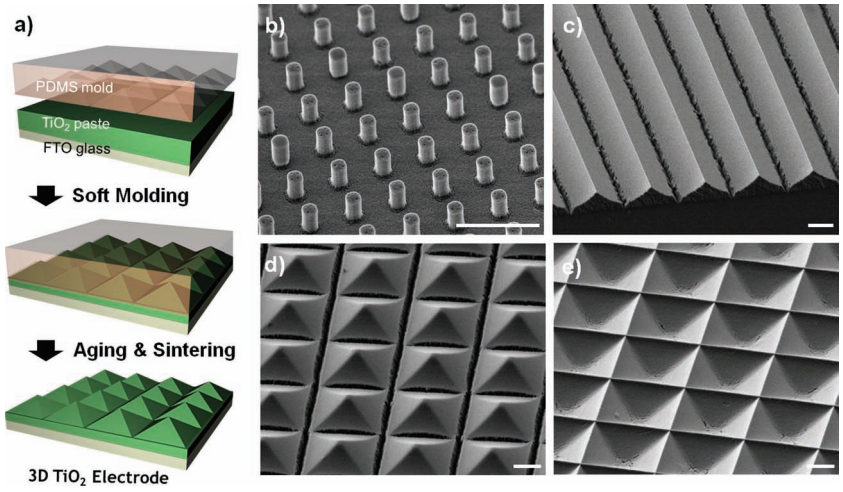

Figure 1. a) A schematic illustration for the fabrication of a 3D TiO_2 photoanode. b–e) SEM images of: b) pillar-, prism-, pyramid-, and inverted-pyramid-patterned TiO_2 photoanodes consisting of 20 nm TiO_2 nanocrystals (scale bars in the SEM pictures: 10 μm).

temperature against the PDMS mold, while guaranteeing full conformal contacts, we annealed the TiO_2 paste film–PDMS mold pair for 10 min at 70 °C to remove residual solvent. The mold was then detached from the patterned TiO_2 film and the partially solidified TiO_2 structure attached to FTO substrate was further sintered at 500 °C for 15 min. The sintered TiO_2 electrode was then dipped into the N719 dyes dissolved in acetonitrile and tert-butanol mixed solvent to let the dye sensitizers be adsorbed on the surface of TiO_2 photoanode. Figure 1b–e show scanning electron microscopy (SEM) images of the patterned TiO_2 photoanodes with pillars (Figure 1b, 2 μm in diameter and 3.5 μm in height), prisms (Figure 1c, 25 μm in width and 11.5 μm in height), pyramids (Figure 1d, 25 μm in width and 12 μm in height), and inverted pyramids (Figure 1e, the same dimensions as the pyramids). It is noted that the feature sizes are in the micrometer-range which is much greater than the wavelength of visible or infrared light. As shown in Figure 1b–e, those patterned electrodes were, indeed, well defined and uniform with TiO_2 nanoparticles over the large surface area (see Supporting Information, Figure S1).

After the soft molding, we compared the absorption properties and photovoltaic performance of the patterned photoanodes with different geometries. The 2D and 3D photoanodes have the same amount of TiO_2 nanoparticles and dye loading, which was confirmed by the dye-loading test after the detachment of the dyes from the TiO_2 films (see Supporting Information, Figure S2). Although the patterned photoanodes adsorbed the same amount of dyes, the 3D photoanodes were found to trap more light than the conventional 2D flat photoanode, as shown in darker red color in **Figure 2**a. Among the 3D photoanodes tested, the pyramid-patterned photoanode traps even more light than the prism-patterned photoanode. The UV–vis absorption spectra, calculated by the measured transmission (T) and reflection (R) (Absorption (%) = 100 – T – R), were obtained with an integrating sphere,[27] as shown in Figure 2b and Figure S3 in

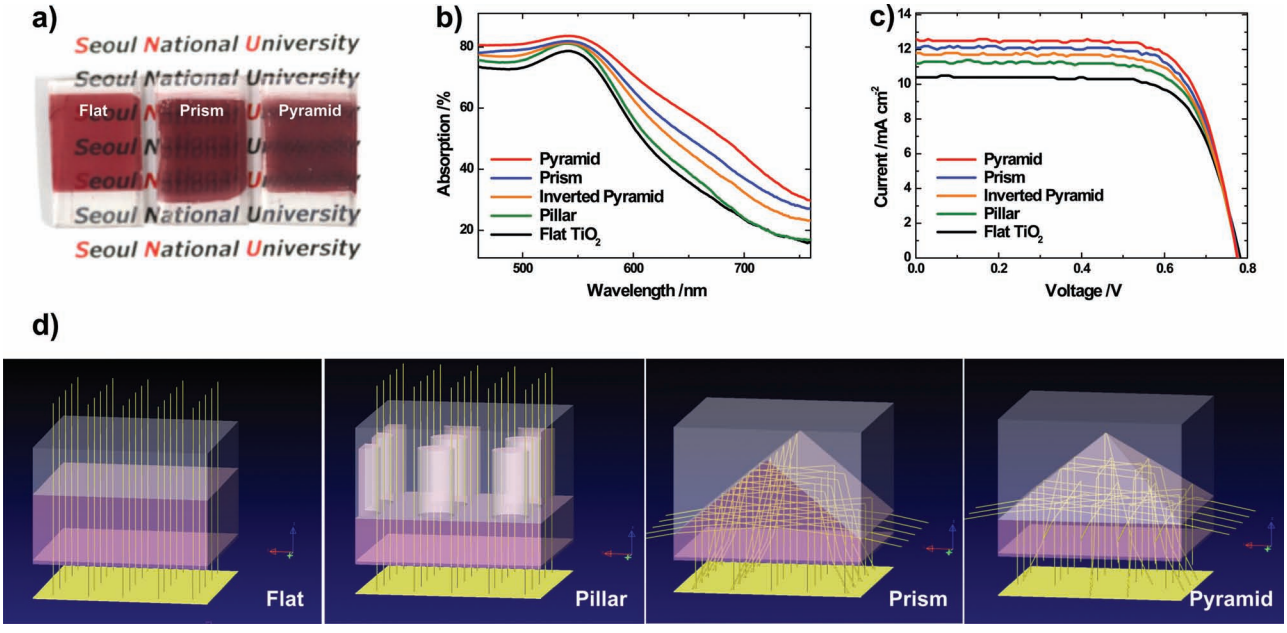

Figure 2. a) A photograph showing 2D (flat), prism-patterned, and pyramid-patterned TiO_2 photoanodes containing N719 dyes. b) Light-absorption characteristics of 2D and 3D TiO_2 photoanodes with different geometries after N719 dye loading, characterized by UV–vis spectroscopy equipped with an integrating sphere. c) The photocurrent–voltage characteristics of DSCs with photoanodes of different geometries, measured under 1 sun illumination (AM 1.5 and 100 mW cm^{-2}) with shading masks (active area: 0.25 cm^2). d) The light path results from the optical simulations with different photoanode geometries with a light source of 650 nm wavelength.

Table 1. Relative absorption data measured by UV–vis spectroscopy and relative optical path lengths calculated by optical simulations for different photoanode geometries or photoanodes combined with scattering layers.

	Wavelength (540 nm)		Wavelength (650 nm)	
	Relative Absorption[a)]	Relative Path Length[b)]	Relative Absorption	Relative Path Length
Flat 2D Photoanode	1	1	1	1
Pillar	1.03	1.005	1.08	1.01
Inverse Pyramid	1.03	1.05	1.27	1.57
Prism	1.04	1.10	1.41	1.76
Pyramid	1.06	1.16	1.62	1.89
Scattering Layer on Flat	1.18	1.21	2.04	2.17
Scattering Layer on Pyramid	1.19	1.24	2.26	2.41

[a)]Relative absorption with reference to the absorption of a flat 2D photoanode, characterized by UV–vis spectroscopy with an integrating sphere; [b)]Relative optical path length with reference to the path length of a flat 2D photoanode calculated by the optical simulation tool.

the Supporting Information. As we anticipated with visual examination of the photoanodes shown in Figure 2a, the 3D photoanodes show the significant increase in absorbance with the enhancement of light trapping capability of the patterned photoanodes. In addition, the pyramid-patterned TiO_2 photoanode has the highest light absorption, compared with other patterned photoanodes. Figure 2c and Figure S4 in the Supporting Information show the photocurrent-voltage (J–V) characteristics of DSCs with photoanodes in different geometries. The pyramid-patterned TiO_2 photoanode represents the highest photocurrent (J_{SC}) as well as the power conversion efficiency (PCE) due to the increased amount of trapped light, as anticipated from the absorption properties.

These light-trapping effects in different geometries of photoanodes are clearly demonstrated in the simulation results obtained using LightTools, a commercial simulation package,[28] as shown in Figure 2d. For the optical simulation, we used the refractive indices of TiO_2 nanostructure containing dyes (including electrolytes within the pores of the TiO_2 nanostructure) and the electrolyte with 2.0 and 1.33, respectively.[29–31] The difference in the refractive index leads to the total reflection on the angled facets of the pyramid-patterned TiO_2 photoanode and the incident light is effectively trapped inside the 3D photoanode. In this aspect, we calculated optical path lengths in different geometries by the ray-tracing method, taking into account dye absorption by the Beer–Lambert law[32] with reference transmittance (15% at 540 nm and 57% at 650 nm wavelength) at the flat 2D photoanode. **Table 1** shows the relative optical path lengths, which are the ratios of optical lengths in the patterned structures to that in the flat photoanode, and relative absorption data. The pyramid-patterned photoanode shows the highest absorption, which is proportional to the optical path length,[3] among the various geometries tested, due to the total reflection on the sloped facets. We note that the experimental and simulation results demonstrating the effective light trapping capability due to the total internal reflection are in good agreement with the analysis with a textured silicon substrate.[3] They compared the light-trapping characteristics for different geometries such as slabs, upright pyramids, and inverted pyramids, demonstrating that the inverted pyramid structures show the highest path-length enhancement. In the case of DSCs, since the incident light is illuminated on a transparent FTO substrate, the effect of inverted pyramids in silicon solar cells is the same as that for the upright-pyramid-patterned photoanodes.

Although the soft-molding method is proven to be quite effective in realizing 3D structures at low cost over a large area, difficulties in preparing 3D pattern masters still exist, due to complicated semiconductor processing or mechanical machining, which is time consuming and expensive. Inspired by the texturing of silicon wafers by wet-etching, we prepared a textured silicon wafer[2] and employed this as a master for PDMS replication. With the PDMS replica molding, we were able to fabricate the randomized pyramid-shaped TiO_2 photoanode in a much simpler and cheaper way, as shown in **Figure 3**a. The texturing of crystalline silicon substrates with anisotropic wet-etching, to have surfaces covered by randomly distributed pyramids of different sizes defined by intersecting (111) crystallographic planes, is a well-known technique.[2] A silicon (100) wafer was etched in an etchant (KOH/isopropyl alcohol (IPA) 10/10 wt% in deionized water) at 70 °C for 40 min. Figure 3b shows an SEM image of the anisotropically etched silicon wafer surface. The pyramidal structures could be therefore easily obtained, with sizes ranging from 1 to 10 μm. We used the anisotropically etched silicon substrate as an original master and replicated it with PDMS to realize a randomized pyramid-shaped TiO_2 photoanode (denoted as R-PY) by the soft molding over a

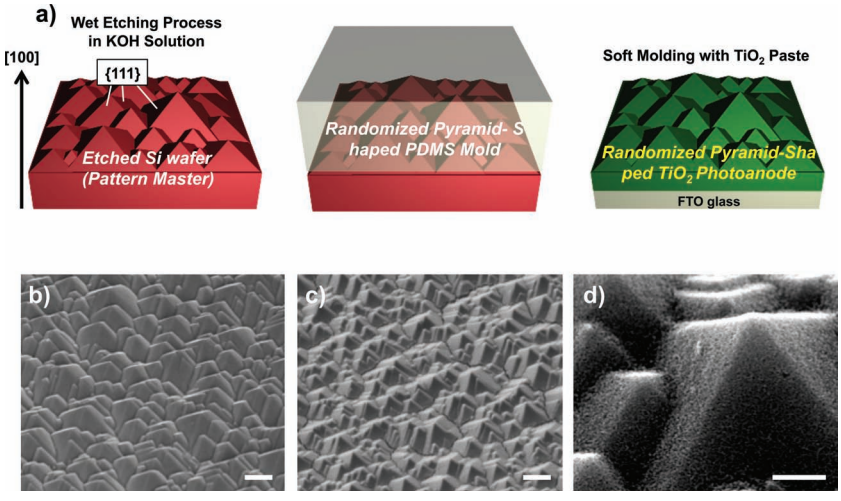

Figure 3. a) A schematic illustration for the fabrication of randomized pyramid-shaped TiO_2 photoanode. b) An SEM image of a randomized pyramid silicon surface, used as a master, fabricated by the anisotropic wet-etching process. c) An SEM image of the randomized pyramid TiO_2 photoanode prepared by replica molding from the silicon master. d) A high-magnification image of the surface in (c). The scale bars in SEM pictures are: 5 μm (b, c), 1 μm (d).

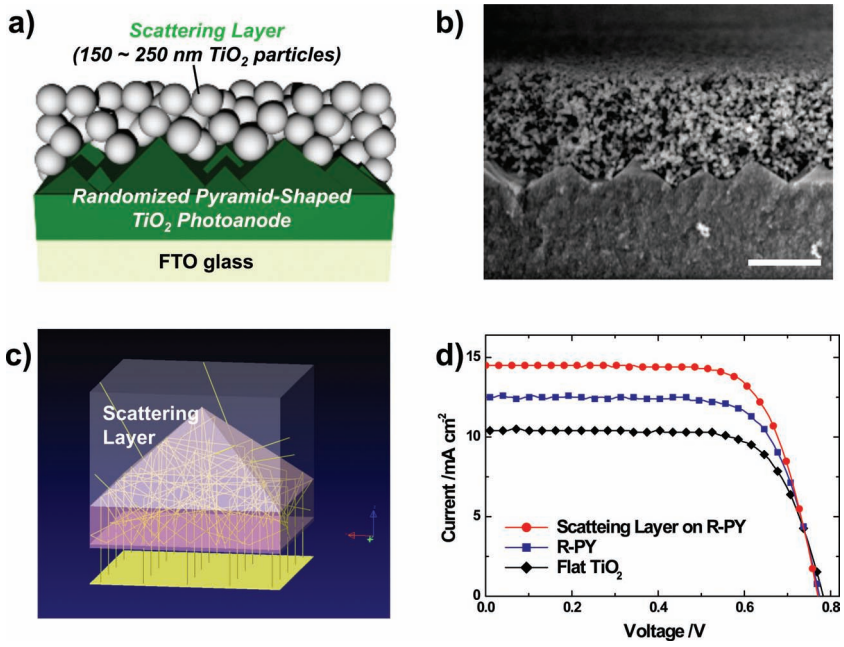

Figure 4. a,b) A schematic illustration (a) and an SEM image (b) of the scattering layer placed on top of the randomized pyramid-patterned TiO_2 photoanode (scale bar in SEM picture: 5 μm). c) An image of ray tracing in the pyramid-shaped photoanode with a scattering layer placed op top, obtained by the optical-simulation tool. d) The photocurrent–voltage characteristics of DSCs with a scattering layer placed on top of a randomized pyramid-patterned TiO_2 photoanode compared with the same characteristics obtained from a flat TiO_2 and a pyramid-patterned photoanode without the scattering layer. They were measured under 1 sun illumination (AM 1.5 and 100 mW cm^{-2}) with shading masks (active area: 0.25 cm^2).

large area. As shown in the SEM image in Figure 3c,d, the TiO_2 photoanode successfully transferred the shape-to-shape of the original silicon master.

To maximize the light trapping in DSCs of the pyramid-patterned photoanode, we extended the strategy by combining a conventional scattering layer method with the 3D R-PY photoanodes (**Figure 4**a). Figure 4b shows the cross-sectional SEM image of a scattering layer consisting of TiO_2 particles in size of 150–250 nm coated on the R-PY photoanode. We note that the scattering layer has low surface area relative to that of TiO_2 photoanodes.[18,24,25] The optical path length was calculated by the ray-tracing method after the patterned photoanode combined with a scattering layer, as shown in Figure 2c. The effect of total reflection on the interface is no longer valid because the refractive indices of the photoanode and the scattering layer are almost the same. On the other hand, the light-scattering effect from scattering particles is increased by the continuous backscattering on the four facets of the pyramid-patterned photoanode structure, and it causes the increase in optical path length over the conventional scattering layer strategy on the flat photoanode as shown in Table 1 and Figure S5 in the Supporting Information. It is noted that the backscattering effect from a scattering layer coated on the patterned photoanode is superior to the effect from the scattering particles incorporated within the photoanode (see Supporting Information, Table S1). The photocurrent-voltage (J–V) characteristics of different types of photoanodes, including the composite photoanode, were obtained under 1 sun conditions (AM 1.5, 100 mW cm^{-2}) with shading masks, as shown in Figure 4d. We note that the R-PY photoanode yields the similar J_{SC} and PCE values when compared with the values obtained from the regularly arranged pyramid photoanode, despite the fact that the R-PY photoanode is fabricated by the much simpler and inexpensive wet-etching process, as summarized in **Table 2**. In particular, a remarkable increase in PCE is achieved by the combination of randomized pyramids with a scattering layer. Especially, we noted that the J_{sc} of DSC was increased over 36% when compared with the conventional 2D flat TiO_2 photoanode because of the enhanced optical light path by backscattering at the surface of the pyramid-patterned photoanodes. This enhancement in the J–V characteristics is also found to agree well with the results of incident photon-to-current efficiency (IPCE) measurement and UV–vis spectra obtained with an integrating sphere, verifying that the enhancement of J–V characteristics is attributed to the extremely efficient light trapping originating from the enhancement of scattering effects on the interface of the pyramid-patterned photoanodes and scattering particles (see Supporting Information, Figure S5).

Further investigations with intensity-modulated photovoltage spectroscopy (IMVS) and intensity-modulated photocurrent spectroscopy (IMPS) indicate that the electron lifetimes and diffusion coefficients are nearly the same for both 2D flat and randomized pyramid-shaped TiO_2 photoanodes (see Supporting Information, Figure S6), corresponding to the measured values of the constant open-circuit voltages (V_{OC}) and fill factors (FF), as shown in Table 2. There is a strong evidence that 3D photoanode structures make light trapping more efficient without giving any deleterious side effects such as the increase in electron recombination.

Table 2. Photovoltaic characteristics of DSCs with photoanodes of different geometries. The sensitizer used was N719 dye; film thickness of flat TiO_2 layer = 7 μm; the electrolyte used was LiI (0.1 M), MPII (0.6 M), I_2 (0.05 M), tBP (0.5 M), and GuSCN (0.05 M) dissolved in acetonitrile; measured under 1 sun illumination (AM 1.5 and 100 mW cm^{-2}) with shading masks (active area = 0.25 cm^2).

	V_{OC} [V]	J_{SC} [mA cm^{-2}]	FF	Efficiency [%]
Flat TiO_2	0.78	10.3	0.73	5.89
Pillar TiO_2	0.78	11.1	0.72	6.13
Prism TiO_2	0.78	12.1	0.72	6.77
Inverted pyramid TiO_2	0.78	11.7	0.72	6.59
Pyramid TiO_2	0.78	12.4	0.73	6.94
R-PY[a)]	0.77	12.5	0.72	6.99
R-PY with a scattering layer	0.78	14.5	0.72	8.02

[a)] R-PY: randomized pyramid-patterned TiO_2 photoanode.

In conclusion, we present a highly efficient and simple light trapping strategy by fabricating novel 3D photoanode to improve the energy conversion efficiency of DSCs. The 3D TiO_2 photoanode structures are prepared by the soft molding method with PDMS molds. Among the different photoanode geometries employed, the pyramid-shaped TiO_2 photoanode shows the highest light absorbance and hense the best photocurrent-voltage performance. From the optical simulation it is noticed that the enhancement of light absorption is caused by the total light reflection off the interfaces between the TiO_2 photoanode and bulk electrolyte. In addition, a simple approach to prepare random pyramid photoanodes at low cost based on the wet-etching of silicon wafers as a master is proposed. Furthermore, we demonstrate the efficient combination strategy of the 3D random pyramid-patterned photoanode with an additional scattering layer and the enhanced photocurrent and power conversion efficiency up to 40% and 36%, respectively, compared with the values for a 2D flat photoanode, are obtained from the increase of the light path length by the reflection of the scattered light on the tilted facets of the pyramid structures.

Experimental Section

Preparation of PDMS Molds for 3D Structures: The pillar-shaped master was produced by conventional photolithography and dry etching process. The prism and pyramid masters used in the present study were prepared mechanically. The detailed procedure can be found elsewhere.[28] After the preparation of the masters, we fabricated the PDMS mold by casting PDMS prepolymer on the master. PDMS precursor with a mixing ratio of 10:1 (precursor:curing agent) was used, and was cured at 60 °C for 10 h. To fabricate the inverse pyramid structure, we used a technique of twice replication with polyurethane acrylate (PUA) (301RM, Minuta Tech). After the preparation of the master, drops of PUA prepolymer mixed with an initiator were dispensed onto the master and a flexible PET film as a supporting plane was placed on top of the liquid prepolymer and was lightly pressed. The prepolymers were then exposed to UV light ($\lambda \approx 250$–400 nm) for several seconds (dose = 100 mJ cm^{-2}) through the reverse side of the transparent PET film for solidification by crosslinking between acrylate functional groups. Then, the cured PUA replica mold on the PET film was removed from the master. For the twice replication, we fabricated PDMS molds by casting on the replicated PUA molds.

Device Fabrication: The electron-blocking layer on the FTO glass was formed by spin-coating 0.1 M of Ti (IV) bis(ethyl acetoacetato)-diisopropoxide dissolved in 1-butanol, then sintering at 500 ºC. Flat, 2D reference TiO_2 electrodes were fabricated by the doctor blade method with TiO_2 paste (DSL 18NR-T, Dyesol) onto the FTO substrate (sheet resistance 8 Ω sq^{-1}, Pilkington). In addition, a paste of 150–250 nm anatase TiO_2 particles (WER2-O, Dyesol) was used as the scattering layer. Above the doctor-blade-coated TiO_2 paste of 7 μm, patterned structures were fabricated by the soft-molding method with the prepared PDMS mold. After pressing the TiO_2 paste at room temperature, samples were annealed at 70 °C for 10 min to remove solvents. The PDMS molds were detached from the patterned TiO_2 microstructures after the first annealing. Then, the solidified TiO_2 electrodes on FTO substrates were sintered at 500 °C for 15 min to entirely remove the organic components of the paste. To adsorb the dye sensitizer, sintered TiO_2 electrodes were dipped in a N719 dye (cis-bis(isothiocyanato)bis(2,2′-bipyridyl-4,4′-dicarboxylato)-ruthenium (II) bis-tetrabutyl ammonium, Dyesol, 0.3 mM) in the acetonitrile and tert-butanol solution (1:1 v/v) at 30 °C for 18 h. Pt counter electrodes were prepared by thermal decomposition of H_2PtCl_6 (0.01 M) in isopropyl alcohol solution spun cast on the FTO substrate at 500 °C for 15 min, and then two holes were made by drill for electrolyte injection. The TiO_2 photoanodes were attached with the counter electrodes using surlyn films (25 μm, Solaronix) which had a role of a spacer between both electrodes. The electrolyte was a mixing solution of 1-methyl-3-propylimidazolium iodide (0.6 M), I_2 (0.05 M), lithium iodide (0.1 M), guanidinium thiocyanate (0.05 M), and 4-tert-butylpyridine (0.5 M) in acetonitrile. This mixed electrolyte was filled into the holes of the Pt counter electrodes of sandwich structured cells by capillary force, and the holes were subsequently sealed by sulyn films and cover glasses.

Optical Simulation: We used a commercial software package (LightTools) for the simulation of optical properties and the calculation of optical path lengths in different structures. The simulation was performed for 7 different structures, such as flat, flat with scattering layer, pillar, inverted pyramid, prism, pyramid, and pyramid with scattering layer, with constant refractive indices of 2.0 for TiO_2 photoanodes, 1.33 for electrolyte layer, and 1.9 for FTO layer.[29–31] Absorption type of TiO_2 layer is assumed by the Beer-Lambert Law with the reference transmittance (15% at 540 nm and 57% at 650 nm wavelength) at the flat 2D photoanode. We used accumulated optical path lengths through optical path length filters on optical receivers of each structure, and calculated the differences between each optical path lengths of filters iteratively. The complete scattering model on boundary surfaces was used for the modeling of the scattering layers of structures with randomized scattering angles in the simulation.

Solar-Cell Characterization: The morphologies of the patterned TiO_2 photoanodes were characterized by field-emission scanning electron microscopy (FE-SEM) using a JSM-5701F (JEOL) instrument. The optical properties of the photoanodes, such as transmission and reflection, were characterized by UV–vis spectroscopy with an integrating sphere (V-670 UV–vis spectrophotometer, Jasco). The current–voltage characterization of the DSCs was carried out using a Keithley 2400 digital source meter and a solar simulator with a 300 W xenon arc-lamp (Newport) under 1 sun illumination (AM 1.5, 100 mW cm^{-2}). On the front side of a FTO substrate, a light-shading mask was applied to clarify an active area of 0.25 cm^2. The external quantum efficiency of the DSCs was analyzed by incident photon to current efficiency measurement (PV measurements, Inc.) as a function of wavelength. The electron lifetimes and electron diffusion coefficients in the TiO_2 electrodes were evaluated by intensity-modulated photovoltage spectroscopy under open-circuit conditions and intensity-modulated photocurrent spectroscopy under short-circuit conditions as a function of light intensity through a controlled intensity modulated photo-spectroscopy system (Zahner) and white-light source (Zahner). The detailed measurement conditions are described elsewhere.[33]

Supporting Information

Supporting information is available from the Wiley Online Library or from the author.

Acknowledgements

This work was financially supported by the National Creative Research Initiative Center for Intelligent Hybrids (No. 2010-0018290) through a National Research Foundation of Korea (NRF) grant, the WCU C2E2 Program (R31-10013), the Basic Science Research Program (2012R1A1A1013688) and the BK21 Program funded by the Ministry of Education, Science, and Technology (MEST) of Korea. Additionally, this work was supported by the Basic Science Research Program through the National Research Foundation of Korea (NRF) grant funded by the Ministry of Education, Science and Technology (MEST) of Korea for the Center for Next Generation Dye-Sensitized Solar Cells (no. 2012-0000591).

Received: January 7, 2013
Revised: March 6, 2013
Published online: May 2, 2013

[1] E. Yablonovitch, *J. Opt. Soc. Am.* **1982**, *72*, 899.
[2] P. Campbell, M. A. Green, *J. Appl. Phys.* **1987**, *62*, 243.
[3] A. W. Smith, A. Rohatgi, *Sol. Energy Mater. Sol. Cells* **1993**, *29*, 37.
[4] H. A. Atwater, A. Polman, *Nat. Mater.* **2010**, *9*, 205.
[5] C. Battaglia, J. Escarré, K. Söderström, M. Charriére, M. Despeisse, F. Haug, C. Ballif, *Nat. Photonics* **2011**, *5*, 535.
[6] J. B. Kim, P. Kim, N. C. Pegard, S. J. Oh, C. R. Kagan, J. W. Fleischer, H. A. Stone, Y.-L. Loo, *Nat. Photonics* **2012**, *6*, 327.
[7] J. Zhu, C. Hsu, Z. Yu, S. Fan, Y. Cui, *Nano Lett.* **2010**, *10*, 1979.
[8] C. Battaglia, J. Escarré, K. Söderström, L. Erni, L. Ding, G. Bugnon, A. Billet, M. Boccard, L. Barraud, S. D. Wolf, F.-J. Haug, M. Dspeisse, C. Bllif, *Nano Lett.* **2010**, *11*, 661.
[9] K. R. Catchpole, S. Mokkapati, F. Beck, E.-C. Wang, A. McKionley, A. Basch, J. Lee, *MRS Bull.* **2011**, *36*, 461.
[10] S. B. Mallick, N. P. Sergeant, M. Agrawal, J. Lee, P. Peumans, *MRS Bull.* **2011**, *36*, 453.
[11] M. Grätzel, *Nature* **2009**, *414*, 338.
[12] M. Grätzel, *Acc. Chem. Res.* **2009**, *42*, 1788.
[13] J. H. Lee, D. W. Kim, H. Jang, J. K. Choi, J. Geng, J. W. Jung, S. C. Yoon, H.-T. Jung, *Small* **2009**, *5*, 2139.
[14] E. S. Kwak, W. Lee, N.-G. Park, J. Kim, H. Lee, *Adv. Funct. Mater.* **2009**, *19*, 1093.
[15] S.-H. Han, S. Lee, H. Shin, H. S. Jung, *Adv. Energy Mater.* **2011**, *1*, 546.
[16] J.-H. Shin, J. H. Moon, *Langmuir* **2011**, *27*, 6311.
[17] S. Ito, S. M. Zakeeruddin, R. Humphry-Baker, P. Liska, R. Charvet, P. Comte, M. K. Nazeeruddin, P. Péchy, M. Takata, H. Miura, S. Uchida, M. Grätzel, *Adv. Mater.* **2006**, *18*, 1202.
[18] S. Hore, C. Vetter, R. Kern, H. Smit, A. Hinsch, *Sol. Energy Mater. Sol. Cells* **2006**, *90*, 1176.
[19] I. Ding, J. Zhu, W. Cai, S. Moon, N. Cai, P. Wang, S. M. Zakeeruddin, M. Grätzel, M. L. Brongersma, Y. Cui, M. D. McGehee, *Adv. Energy Mater.* **2011**, *1*, 52.
[20] S. M. Kong, Y. Xiao, K. H. Kim, W. I. Lee, C. W. Chung, *Thin Solid Films* **2011**, *519*, 3173.
[21] F. Wang, N. K. Subbaiyan, Q. Wang, C. Rochford, G. Xu, R. Lu, A. Elliot, F. D'Souza, R. Hui, J. Wu, *ACS Appl. Mater. Interfaces* **2012**, *4*, 1565.
[22] J. Kim, J. K. Koh, B. Kim, J. H. Kim, E. Kim, *Angew. Chem. Int. Ed.* **2012**, *51*, 6864.
[23] Y. S. Kim, K. Y. Suh, H. H. Lee, *Appl. Phys. Lett.* **2001**, *79*, 2285.
[24] Z.-S. Wang, H. Kawauchi, T. Kashima, H. Arakawa, *Coord. Chem. Rev.* **2004**, *248*, 1381.
[25] Y. Chiba, A. Islam, Y. Watanabe, R. Komiya, N. Koide, L. Han, *Jpn. J. Appl. Phys.* **2006**, *45*, L638.
[26] S. J. Choi, P. J. Yoo, S. J. Baek, T. W. Kim, H. H. Lee, *J. Am. Chem. Soc.* **2004**, *126*, 7744.
[27] M. D. Brown, T. Suteewong, R. S. S. Kumar, V. D'Innocenzo, A. Petrozza, M. M. Lee, U. Wiesner, H. J. Snaith, *Nano Lett.* **2011**, *11*, 438.
[28] H. Yoon, S. G. Oh, D. S. Kang, J. M. Park, S. J. Choi, K. Y. Suh, K. Char, H. H. Lee, *Nat. Commun.* **2011**, *2*, 455.
[29] A. Mihi, F. J. López-Alcaraz, H. Miguez, *Appl. Phys. Lett.* **2006**, *88*, 193110.
[30] F. Wang, N. K. Subbaiyan, Q. Wang, C. Rochford, G. Xu, R. Lu, A. Elliot, F. D'Souza, R. Hui, J. Wu, *ACS Appl. Mater. Interfaces* **2012**, *4*, 1565.
[31] A. Mihi, C. Zhang, P. V. Braun, *Angew. Chem. Int. Ed.* **2011**, *50*, 5712.
[32] F. L. Pedrotti, L. M. Pedrotti, L. S. Pedrotti, *Introduction to Optics, 3rd ed.*, Pearson/Prentice Hall, LondonUK, **2007**.
[33] L. M. Peter, K. G. U. Wijayantha, *Electrochim. Acta* **2000**, *45*, 4543.